14-3-3εa directs the pulsatile transport of basal factors toward the apical domain for lumen growth in tubulogenesis

Yuji Mizotani[a], Mayu Suzuki[a], Kohji Hotta[a,1], Hidenori Watanabe[b], Kogiku Shiba[c], Kazuo Inaba[c], Etsu Tashiro[a], Kotaro Oka[a], and Masaya Imoto[a,1]

[a]Department of Biosciences and Informatics, Faculty of Science and Technology, Keio University, 223-8522 Yokohama, Japan; [b]Graduate School of Agricultural and Life Sciences, The University of Tokyo, 113-8657 Tokyo, Japan; and [c]Shimoda Marine Research Center, University of Tsukuba, 415-0025 Shizuoka, Japan

Edited by Satyajit Mayor, National Centre for Biological Sciences, Bangalore, India, and approved August 8, 2018 (received for review May 22, 2018)

The *Ciona* notochord has emerged as a simple and tractable in vivo model for tubulogenesis. Here, using a chemical genetics approach, we identified UTKO1 as a selective small molecule inhibitor of notochord tubulogenesis. We identified 14-3-3εa protein as a direct binding partner of UTKO1 and showed that 14-3-3εa knockdown leads to failure of notochord tubulogenesis. We found that UTKO1 prevents 14-3-3εa from interacting with ezrin/radixin/moesin (ERM), which is required for notochord tubulogenesis, suggesting that interactions between 14-3-3εa and ERM play a key role in regulating the early steps of tubulogenesis. Using live imaging, we found that, as lumens begin to open between neighboring cells, 14-3-3εa and ERM are highly colocalized at the basal cortex where they undergo cycles of accumulation and disappearance. Interestingly, the disappearance of 14-3-3εa and ERM during each cycle is tightly correlated with a transient flow of 14-3-3εa, ERM, myosin II, and other cytoplasmic elements from the basal surface toward the lumen-facing apical domain, which is often accompanied by visible changes in lumen architecture. Both pulsatile flow and lumen formation are abolished in larvae treated with UTKO1, in larvae depleted of either 14-3-3εa or ERM, or in larvae expressing a truncated form of 14-3-3εa that lacks the ability to interact with ERM. These results suggest that 14-3-3εa and ERM interact at the basal cortex to direct pulsatile basal accumulation and basal–apical transport of factors that are essential for lumen formation. We propose that similar mechanisms may underlie or may contribute to lumen formation in tubulogenesis in other systems.

14-3-3 | ERM | tubulogenesis | pulsatile directed flow | myosin II

Biological tubes serve as fundamental structural units in a diverse set of organs, including lung, liver, gut, and kidney, playing roles in both the exchange of biological materials and structural support. Tubulogenesis involves changes in cell shape (1–5), vesicle trafficking (6–11), and luminogenesis (12–15). Understanding how these changes occur and how they are coordinated in space and time is essential for understanding tubulogenesis during normal development and is also becoming increasingly important for regenerative medicine.

The notochord of *Ciona robusta* provides a simple in vivo model for tubulogenesis. The ascidian notochord initially comprises a single stack of 40 postmitotic cells that form the core of the tadpole tail. As the notochord begins to elongate along its anterior/posterior (AP) axis (16–18), extracellular lumen pockets emerge between adjacent cells, expand, and fuse with each other to form a single central lumen (19–21). Although this process has been extensively characterized, the underlying mechanisms remain poorly understood. Recent studies have revealed molecules that are associated with both notochord elongation and tubulogenesis. For example, cell elongation is facilitated by actomyosin networks (complexes of actin and myosin II) localizing in the basal contractile ring, together with other components such as α-actinin and cofilin (20, 22). Lumen formation requires the establishment of polarity by Par3/Par6/aPKC (23) and the cytoskeletal cross-linker ezrin/radixin/moesin (ERM) (20), both of which play roles in other tubulogenesis processes, including those occurring in Madin–Darby canine kidney (MDCK) cells (6, 24, 25), the *Drosophila* trachea (4, 11), and the *Caenorhabditis elegans* intestine (12, 26). However, it remains largely unknown how these molecules work together or how cell elongation and lumen formation combine, suggesting that there are novel mediators that affect these genes.

One of the best approaches for elucidating the molecular mechanisms underlying biological processes is a chemical genetics approach utilizing chemical inhibitors. The compounds identified from phenotypic screening have previously led us to identify unexpected molecules responsible for various phenotypes. Furthermore, such compounds enable us to examine the functional role of the target molecule just by changing their treatment time or concentration. This chemical genetics strategy has been useful not only to in vitro cell biology (27, 28), but also

Significance

Ascidians have become a powerful model system in which to uncover basic mechanisms that govern body plan specification and elaboration. In particular, the ascidian notochord is a highly tractable model for tubulogenesis. Here, we use chemical genetics to identify roles for 14-3-3εa, and its binding partner ezrin/radixin/moesin (ERM), in tubulogenesis. Combining genetic and chemical perturbations with live cell imaging, we present evidence that 14-3-3εa–ERM interactions are required for tubulogenesis and that they act by promoting a directed cytoplasmic flow, previously uncharacterized, which carries lumen-associated components from the basal domain to the apical domain to feed lumen growth. Because many core components of this system are highly conserved, these results have broad implications for tubulogenesis in many other contexts.

Author contributions: Y.M., M.S., K.H., and M.I. designed research; Y.M. and M.S. performed research; K.H., H.W., K.S., K.I., and K.O. contributed new reagents/analytic tools; H.W., K.S., K.I., and E.T. analyzed data; Y.M., K.H., E.T., and M.I. wrote the paper; and K.O. and M.I. supervised research.

The authors declare no conflict of interest.

This article is a PNAS Direct Submission.

Data deposition: The following genes have been deposited in the GenBank database: 14-3-3εa (accession no. LC318447), 14-3-3εb (accession no. LC318448), 14-3-3γ1 (accession no. LC318449), 14-3-3γ2 (accession no. LC318450), ERM (accession no. NM_001032427), and myosin II (accession no. XM_002123773).

[1]To whom correspondence may be addressed. Email: khotta@bio.keio.ac.jp or imoto@bio.keio.ac.jp.

This article contains supporting information online at www.pnas.org/lookup/suppl/doi:10.1073/pnas.1808756115/-/DCSupplemental.

Published online August 29, 2018.

to in vivo developmental biology (29, 30). Here, we demonstrate an in vivo chemical biological approach to identify molecules responsible for tubulogenesis and to elucidate their functional roles in vivo. We identify a chemical inhibitor of tubulogenesis in *C. robusta*. We identify its target protein 14-3-3εa, and we show that 14-3-3εa interacts with ERM during lumen formation to control dynamic cycles of basal accumulation and directed transport of 14-3-3εa, ERM, myosin II, and other factors from the basal cortex to the lumen-facing apical domain and to promote lumen formation and growth during tubulogenesis.

Results

UTKO1 Was Found to Inhibit Notochord Tubulogenesis Using Unbiased Phenotypic Screening. We began by conducting a phenotypic screen to identify compounds that modulate the morphogenesis of *C. robusta*. Embryos of *C. robusta* reach the tailbud stage at 12 h postfertilization (hpf) and become swimming larvae at 21 hpf, at which point they possess their maximum tail length (31). We treated *C. robusta* embryos at 12 hpf with compounds from our in-house chemical library and assessed their effects on subsequent development. We found that UTKO1, a tumor cell migration inhibitor we developed previously (32, 33), inhibits tail elongation in a dose-dependent manner (*SI Appendix*, Fig. S1 *A* and *B*). Interestingly, UTKO1 did not appear to cause any noticeable morphological defects in other body parts, such as the trunk (*SI Appendix*, Fig. S1*C*), or defects in other developmental processes, such as ocellus melanization (*SI Appendix*, Fig. S1*D*), although it did cause defects in papillae formation and locomotion (*SI Appendix*, Fig. S1*E* and Movie S1).

The tail-selective phenotype resulting from UTKO1 treatment prompted us to look more closely at the dynamics of notochord elongation and tubulogenesis in UTKO1-treated embryos. Notochord elongation and tubulogenesis involves four distinct developmental phases (Fig. 1): (phase I) completion of notochord cell alignment into a single file and elongation of notochord cells along the AP axis; (phase II) opening of small extracellular lumen pockets between adjacent notochord cells; (phase III) expansion of the lumen pockets, accompanied by crawling movements of the notochord cells; and (phase IV) connection of the lumen pockets to form a single lumen at the center of the notochord tube (1). Treatment with UTKO1 caused a concentration-dependent delay in the opening and expansion of the lumen, relative to untreated controls (Fig. 1 and *SI Appendix*, Fig. S1*F*). However, this inhibitory effect of UTKO1 was not observed when it was added at 16 hpf (*SI Appendix*, Fig. S1*G*), suggesting that UTKO1 selectively inhibits phases I and II, which occur from 12 to 16 hpf. Thus, UTKO1 was found to inhibit lumen formation in *Ciona* notochord during the early stages of tubulogenesis.

14-3-3εa Is a Direct Target of UTKO1 in *Ciona*. To identify the moiety of UTKO1 required for its inhibitory activity, we performed a structure–activity relationship (SAR) analysis using UTKO1 analogs that we had previously synthesized (32). Analogs that lacked the hydroxyl group present at C-11 of UTKO1 (UTKO9, UTKO10, UTKO13, UTKO14, and UTKO16) or the methylene group at C-4 (UTKO7), did not inhibit tubulogenesis, suggesting that these two groups are critical for inhibitory activity (Fig. 2*A* and *SI Appendix*, Fig. S2 *A* and *C*). In contrast, an analog that lacks the aldehyde group (UTKO12) and four stereoisomers of UTKO1 retained inhibitory activity (Fig. 2*A* and *SI Appendix*, Fig. S2 *B* and *D*), indicating that the aldehyde group and a specific 3D shape are not required to inhibit tubulogenesis.

Based on these results, we used a UTKO1 analog in which the aldehyde group is replaced by biotin (B-UTKO1ox) (Fig. 2*B*), to identify target proteins in *Ciona* lysates that bind UTKO1. Previously, we showed that UTKO1 targets human 14-3-3ζ protein (33), an adapter protein that binds to diverse client proteins (34, 35). Therefore, we used the human anti–14-3-3 antibody as a probe for the UTKO1 target proteins in *C. robusta*. Proteins that bind to the human anti–14-3-3 antibody were pulled down from the *Ciona* lysate by B-UTKO1ox (Fig. 2*C*), suggesting that UTKO1 targets one or more of the four isoforms of *Ciona* 14-3-3: εa, εb, γ1, and/or γ2. To identify the specific target(s), we prepared each 14-3-3 isoform as a recombinant protein fused to GST and tested for direct binding to B-UTKO1ox. As shown in Fig. 2*D*, among the four *Ciona* 14-3-3 isoforms, only 14-3-3εa was strongly pulled down by B-UTKO1ox, and biotin-free UTKO1 inhibited the interaction (Fig. 2*E*). Conversely, a UTKO1 analog that lacked the C-11 hydroxyl group (UTKO10) did not show the same pattern. Unlike B-UTKO1ox, B-UTKO1ph did not strongly pull down GST-14-3-3εa (Fig. 2*F*). These results suggest that UTKO1 binds directly and selectively to 14-3-3εa via the hydroxyl group at C-11, which is important for its inhibitory activity against tubulogenesis. This selective binding of UTKO1 to 14-3-3εa allowed us to explore the functional role of 14-3-3εa in lumen formation during *Ciona* tubulogenesis.

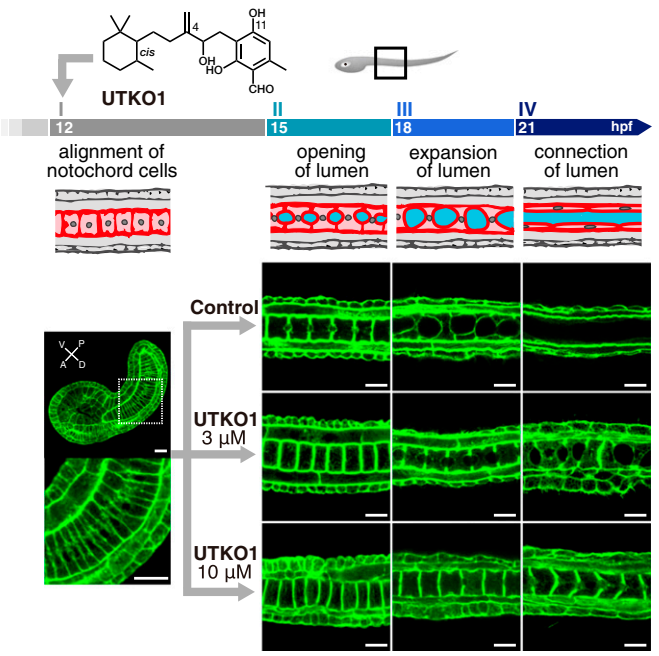

Fig. 1. UTKO1 inhibits tubulogenesis in the *Ciona* notochord. Schematic illustrations and confocal images of *Ciona* tails treated with or without UTKO1 during notochord tubulogenesis. Notochord cells are colored red, and lumens are blue. Confocal images were obtained by staining F-actin with Alexa Fluor 488 phalloidin. A, anterior; D, dorsal; P, posterior; V, ventral. (Scale bars: 10 μm.)

14-3-3εa Is Required for Notochord Tubulogenesis. The 14-3-3εa mRNA was highly expressed during notochord tubulogenesis and peaked at 15 hpf (*SI Appendix*, Fig. S3*A*). To investigate the role of 14-3-3εa, we injected a morpholino antisense oligonucleotide (MO) directed against 14-3-3εa into fertilized eggs, to inhibit the synthesis of 14-3-3εa protein, starting from the fertilized egg stage. Treatment with 14-3-3εa MO caused a tail elongation defect that could be detected as early as 12 hpf and increased in severity as development progressed, up until 21 hpf (*SI Appendix*, Fig. S1 *H* and *I*). At 21 hpf, larvae treated with 14-3-3εa MO exhibited a failure of lumen opening or expansion, as seen with UTKO1 treatment (Fig. 2 *G–I* and *SI Appendix*, Fig. S1*K*). On the other hand, 14-3-3εa MO also caused defects in trunk development (*SI Appendix*, Fig. S1*J*), consistent with the 14-3-3εa expression pattern in the trunk (36, 37) (*SI Appendix*, Fig. S3*D*). The tail defects, but not trunk defects, were rescued by the notochord-specific expression of MO-resistant 14-3-3εa, driven by a notochord-specific brachyury promoter (Fig. 2*J* and *SI Appendix*, Fig. S1 *H–K*),

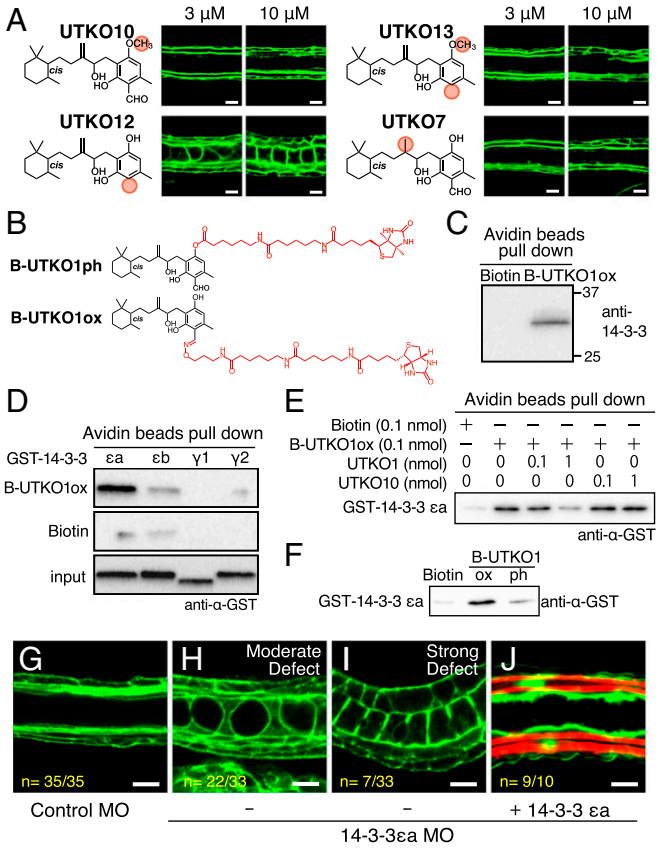

Fig. 2. 14-3-3εa, a target of UTKO1, is required for tubulogenesis in *Ciona* notochord. (*A*) Structure–activity relationship (SAR) of UTKO1 analogs. Red circles indicate the alterations to UTKO1. The phenotype resulting from treatment with each compound is shown in the confocal images, with Alexa 488 phalloidin staining for F-actin. (*B*) Structure of two biotinylated versions of UTKO1: B-UTKO1ph and B-UTKO1ox. (*C*) *Ciona* lysate was incubated with biotin (1 nmol) or B-UTKO1ox (1 nmol), precipitated with avidin beads, and subjected to SDS/PAGE. (*D*) Purified GST-tagged 14-3-3 isoforms were incubated with B-UTKO1ox or biotin, precipitated with avidin beads, and subjected to SDS/PAGE. (*E*) GST-14-3-3εa was incubated with UTKO1 or UTKO10 before precipitation with biotin or B-UTKO1ox, using avidin beads. The precipitated proteins were subjected to SDS/PAGE. (*F*) Purified GST-tagged 14-3-3 isoforms were incubated with biotin, B-UTKO1ox, or B-UTKO1ph, precipitated with avidin beads, and subjected to SDS/PAGE. (*G–J*) Confocal images of *Ciona* larvae at 21 hpf injected with Control MO (*G*), 14-3-3εa MO (*H* and *I*), and 14-3-3εa MO + 14-3-3εa:EGFP expressed from the Brachyury promoter (Bra>14-3-3εa:EGFP) (*J*). Confocal images of F-actin stained with Alexa 488 phalloidin (green) (*G–I*) or Alexa 594 phalloidin (red) (*J*). In *J*, GFP-14-3-3εa was further stained with anti-GFP (green). (Scale bars: 10 μm.)

confirming that UTKO1 inhibits notochord lumen formation by binding to 14-3-3εa.

14-3-3εa Interacts Directly with Ezrin/Radixin/Moesin. We hypothesized that UTKO1 exerts its inhibitory effects by preventing 14-3-3εa from binding to one or more client proteins responsible for notochord lumen formation. Since UTKO1 showed greater selectivity toward notochord cells (*SI Appendix*, Fig. S1 *B* and *C*) relative to 14-3-3εa MO treatment (*SI Appendix*, Fig. S1 *I* and *J*), we focused on potential clients that are predominantly expressed in notochord cells during tubulogenesis (38, 39). Of these, ezrin/radixin/moesin (ERM) is the most likely candidate, since it is required for lumen formation during *Ciona* notochord development (20), as well as in other tubulogenesis processes (6), and was recently reported to interact directly with the 14-3-3 protein in human cell lines to regulate cell migration (40).

Indeed, ERM protein purified from *E. coli* bound 14-3-3 protein from *Ciona* lysate, detected by anti–14-3-3 (Fig. 3*A*), and also bound 14-3-3εa purified from *E. coli* (Fig. 3*B*), supporting a direct interaction between 14-3-3εa and ERM in *Ciona*. Furthermore, the interaction between 14-3-3εa and ERM was inhibited in a dose-dependent manner by UTKO1 (Fig. 3*B*), but not by an off-targeted derivative, UTKO10 (Fig. 3*C*). Deletion mutants of 14-3-3εa lacking amino acids 156 to 206 did not bind to ERM or B-UTKO1ox (Fig. 3 *D–F*), indicating that ERM and UTKO1 bind to the same 156- to 206-aa domain. This domain corresponds to the ezrin binding domain in human 14-3-3ζ (40), suggesting the existence of a conserved interaction across species. Together, these results implicate ERM as a 14-3-3εa client protein that mediates the effects of 14-3-3εa on notochord tubulogenesis.

14-3-3εa and ERM Colocalize in the Basal Contractile Ring. Immunostaining using specific antibodies (*SI Appendix*, Fig. S3 *B* and *C*) revealed that 14-3-3εa was ubiquitously expressed in various cell types, including notochord, epidermis, muscle, and neuronal cells (Fig. 3*G* and *SI Appendix*, Fig. S3*D*). On the other hand, ERM was almost exclusively expressed in the notochord, with lower levels in the neural tube and in some neuronal cells in the trunk region. Focusing on notochord cells, 14-3-3εa and ERM were strongly colocalized in the basal contractile ring, an actomyosin-based contractile ring that forms on the basal surface of notochord cells during notochord elongation and lumen opening at 15 hpf (Fig. 3*G*, arrowheads). In larvae treated with UTKO1, ERM was still localized in the basal contractile ring, but coenrichment of 14-3-3εa at the same location was greatly reduced (Fig. 3*H*). Since UTKO1 did not affect the amount of 14-3-3εa protein expression (*SI Appendix*, Fig. S3*C*), the disappearance of 14-3-3εa from the basal contractile ring in notochord cells reflects its delocalization due to loss of binding to ERM. We conclude that UTKO1 inhibits the colocalization of 14-3-3εa with ERM in the basal contractile ring, by inhibiting their direct interaction in the notochord.

14-3-3εa and ERM Undergo Cycles of Basal Accumulation Followed by Basal–Apical Transport. To investigate how the colocalization of 14-3-3εa and ERM in the basal contractile ring is related to lumen formation, we performed live imaging of each protein fused with a fluorescent protein under a brachyury promoter. Just before phase II (the lumen opening) (Fig. 1) at 15 hpf, we observed coaccumulation of 14-3-3εa and ERM in the basal contractile ring (Fig. 4*A* and Movie S2), consistent with the results of immunostaining (Fig. 3*G*). During phase II (15 to 17 hpf), a behavior emerged in which 14-3-3εa and ERM periodically appeared and then disappeared from the basal contractile ring (Fig. 4 *B* and *D*, and Movie S3).

To test whether the disappearance of 14-3-3εa and ERM from the basal cortex during each cycle is associated with their accumulation elsewhere, we used spatiotemporal cross-correlation analysis to identify other cellular regions that show increases in 14-3-3εa or ERM signal intensity that correlate with the disappearance from the basal cortex. Significantly, we found that increases in 14-3-3εa and ERM signal intensities in the apical domain were highly correlated with decreases in the basal domain during each cycle, with a consistent peak time lag (0.8 to 1.2 min) (Fig. 4*H*). This suggests that 14-3-3εa and ERM are translocated from the basal to apical domain during each cycle. Indeed, immunostaining of 14-3-3εa and ERM at 18 hpf, 3 h after the initiation of phase II, revealed strong apical enrichment (*SI Appendix*, Fig. S3*E*).

Indeed, by live imaging (Movie S3), we could detect rapid movements of vesicles containing 14-3-3εa and ERM into the apical domain following their disappearance from the basal cortex, sometimes accompanied by visible changes in lumen architecture and size (Fig. 4 *J* and *K*). Interestingly, this translocation

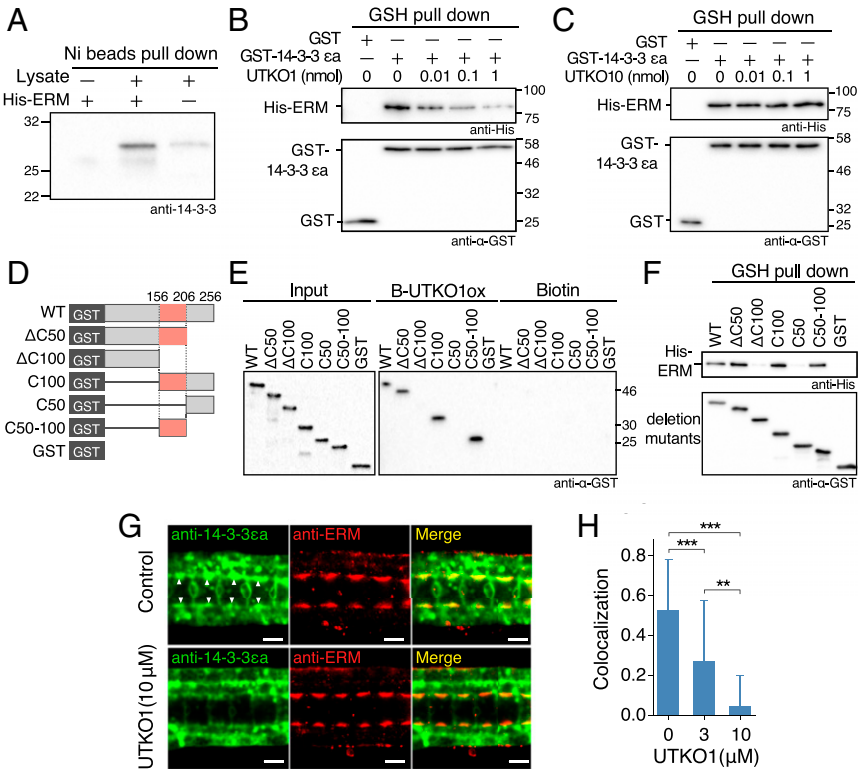

Fig. 3. UTKO1 inhibits 14-3-3εa interacting and colocalizing with ERM. (*A*) His-tagged ERM was purified from *E. coli* and mixed with *Ciona* lysate. His-ERM–binding proteins were captured using Ni-beads, eluted with imidazole, and subjected to SDS/PAGE. (*B* and *C*) Purified His-tagged ERM protein was preincubated with or without UTKO1/UTKO10, mixed with GST/GST14-3-3εa, precipitated with glutathione–sepharose (GSH) beads, and subjected to SDS/PAGE. (*D*) Schematic illustrations of deletion mutants of 14-3-3εa purified from the *E. coli* BL21 strain. (*E*) Deletion mutants of GST-14-3-3εa were incubated with B-UTKO1ox or biotin, precipitated with avidin beads, and subjected to SDS/PAGE. (*F*) Purified His-tagged ERM protein was mixed with GST-14-3-3 deletion mutants, precipitated by GSH beads, and subjected to SDS/PAGE. (*G*) Confocal images of the immunostaining of 14-3-3εa (green), ERM (red), and the merged image at 15 hpf in the control and UTKO1 (10 μM)-treated larvae. White arrowheads indicate the accumulation of 14-3-3εa in the basal contractile ring. (Scale bars: 10 μm.) (*H*) Colocalizations between 14-3-3εa and ERM, expressed as Pearson's coefficients, measured for the basal contractile rings. Data presented as mean ± SD (n = 31, 21, and 18 for UTKO1 0 μM, 3 μM, and 10 μM, respectively; $^{**}P < 0.05$; $^{***}P < 0.001$; Bonferroni multiple comparison test).

of 14-3-3εa and ERM was accompanied by the basal-to-apical movement of cytoplasmic elements, visualized using differential interference contrast (DIC) optics (Fig. 4*L* and Movie S3), suggesting that a bulk cytoplasmic flow may carry 14-3-3εa and ERM from the basal contractile ring to the apical domain.

Interaction Between 14-3-3εa and ERM Is Required for Their Pulsatile Accumulation and Basal–Apical Translocation. In larvae treated with high doses (10 μM) of UTKO1, the pulsatile accumulations of 14-3-3εa and ERM were abolished (Fig. 4 *C* and *F*), and we could no longer detect obvious directed basal–apical movements of 14-3-3εa, ERM, or other cytoplasmic elements (Movie S4) or significant correlations between the apical and basal intensities of 14-3-3εa and ERM (Fig. 4*I*). At intermediate doses of UTKO1 (3 μM), pulsatile accumulations of 14-3-3εa and ERM persisted, but the time between pulses was increased relative to untreated controls (Fig. 4 *E* and *G*). Supporting these live imaging results, treatment with UTKO1 also inhibited the apical accumulation of ERM at 18 hpf in fixed immunostained embryos (*SI Appendix*, Fig. S3 *F* and *G*).

These results suggest that an interaction between 14-3-3εa and ERM is required for their pulsatile accumulation and basal–apical translocation. To test this further, we first examined localization of 14-3-3εa in ERM KD embryos, and ERM in 14-3-3εa KD embryos, focusing initially at 15 hpf, when lumen opening is about to begin in the WT. ERM localized normally to the basal contractile ring in 14-3-3εa knocked-down (KD) embryos (Fig. 5*A* and Movie S5) while 14-3-3εa failed to target the basal contractile ring in ERM KD embryos (Fig. 5*B* and Movie S6). A truncated form of 14-3-3εa (14-3-3εaΔC50-100), that cannot interact with ERM, also failed to localize to the basal contractile ring when expressed in place of endogenous 14-3-3εa (Fig. 5*C* and Movie S7). Thus, 14-3-3εa is not required for accumulation of ERM in the basal contractile ring while the accumulation of 14-3-3εa in the basal contractile ring depends on its ability to interact with ERM. These results are consistent with the diminished accumulation of 14-3-3εa, but not ERM, in the basal contractile ring with UTKO1 treatment (Fig. 3*G*).

We next examined pulsatile accumulation and translocation of 14-3-3εa or ERM during phase II (15 to 17 hpf) in ERM KD, 14-3-3εa KD, and 14-3-3εaΔC50-100–expressing embryos. We found that pulsatile accumulation of 14-3-3εa (or 14-3-3εaΔC50-100) in the basal contractile ring was abolished in ERM KD or 14-3-3εaΔC50-100–expressing embryos. Conversely, pulsatile accumulation of ERM was abolished in 14-3-3εa KD embryos. Under all three perturbations, basal–apical flows of cytoplasm observed by DIC were severely attenuated, correlations between basal and apical accumulations of either 14-3-3εa or ERM were severely attenuated, and lumens failed to form and grow [Control (Fig. 5*D* and Movie S8); 14-3-3εa KD (Fig. 5*E* and Movie S9); ERM KD (Fig. 5*F* and Movie S10); and 14-3-3εaΔC50-100 (Fig. 5*G* and Movie S11)]. These results suggest that local interactions between 14-3-3εa and ERM at the basal cortex are required for their pulsatile basal accumulation, directed transport toward the apical/luminal domain, and lumen formation and growth.

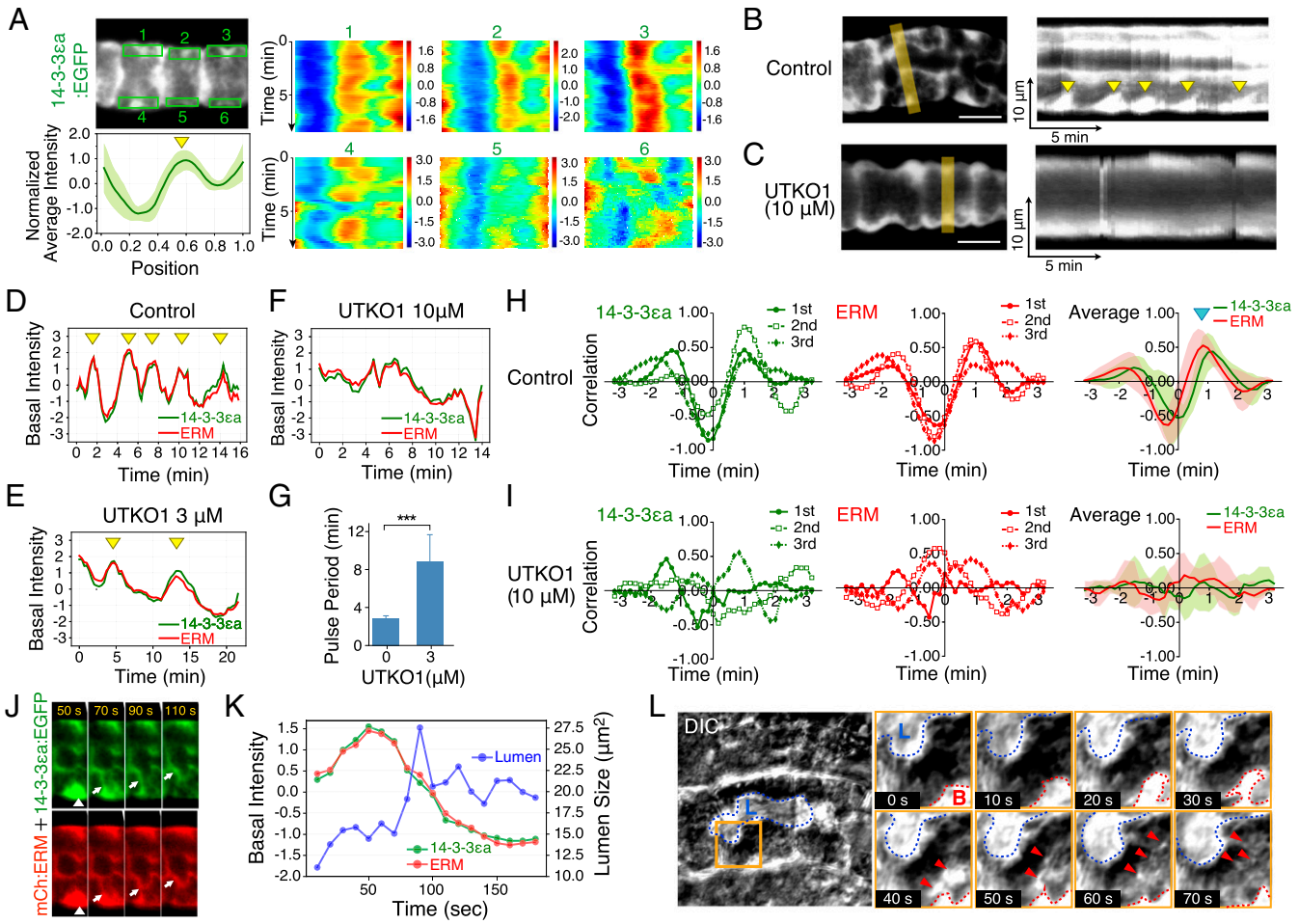

Fig. 4. Pulsatile basal accumulation and basal–apical translocation lead to the accumulation of 14-3-3εa and ERM in the lumen-facing apical domain during lumen growth. (*A*) Live imaging and the quantification of 14-3-3εa:EGFP just before phase II (15 hpf). The intensities in region of interest (ROI) (shown in green) were quantified, normalized along the AP axis, and displayed as a kymograph. The total intensities of all ROIs and time points were plotted along the relative position of the AP axis. The yellow arrowhead indicates the accumulation of 14-3-3εa:EGFP in the basal contractile ring, the middle position of the basal domain. (*B* and *C*) Kymograph analysis of the dynamics of 14-3-3εa during phase II (15 to 17 hpf) in a control (*B*) and when treated with UTKO1 (10 μM) (*C*) from 12 hpf. The placement of the cross-sections used to generate the kymograph is indicated by yellow bands. Yellow triangles indicate the pulsed accumulation of 14-3-3εa. (Scale bars: 10 μm.) (*D*–*F*) The intensity of 14-3-3εa and ERM in the basal contractile ring over time during phase II (15 to 17 hpf) in the larva treated with control (*D*), UTKO1 3 μM (*E*), and UTKO 10 μM (*F*). Yellow arrowheads indicate the pulsatile accumulation of 14-3-3εa and ERM. (*G*) The pulse period of 14-3-3εa in the basal contractile ring during phase II calculated in the control and UTKO1 3 μM-treated larva. Data are presented as mean ± SD (nine cycles for three cells for control, and seven cycles for four cells for UTKO1 3 μM; ***$P < 0.001$; two-tailed t test). In UTKO 1 10 μM, pulses were not observed. (*H* and *I*) Cross-correlation analysis between the signal of the basal contractile ring and apical domain in control (*H*) and UTKO1 (10 μM)-treated larva (*I*). The cross-correlation function was calculated for three cycles individually for 14-3-3εa (*Left*) and ERM (*Middle*), and their averages were plotted, with shading representing the SD (*Right*). The blue arrowhead indicates the peak, the shift of which indicates a high correlation between the basal contractile ring and the apical domain. (*J*) Live imaging of 14-3-3εa:EGFP and mCherry:ERM during their apical translocation. White arrowheads indicate the basal contractile ring, and white arrows indicate the internalizing of 14-3-3εa or ERM toward the apical domain. (*K*) Quantification of the signal intensity of 14-3-3εa and ERM in the basal contractile ring, and (*I*) the size of lumen over time. (*L*) DIC images during lumen formation. Blue dotted lines indicate the lumen area, red dotted lines indicate inflation of the cytoplasmic region containing basal factors, and red triangles show the region rushing into the apical domain.

Pulsatile Basal Accumulation and Basal–Apical Transport of 14-3-3εa and ERM Are Closely Associated with Those of Myosin II. We next asked whether pulsatile basal accumulation and basal–apical transport of 14-3-3εa and ERM are associated with movements of other cortical elements. We focused on nonmuscle myosin II, which is known to be enriched in the basal contractile ring and interacts with actin filaments to promote actomyosin contractility that is critical for notochord cell elongation along the AP axis, and is also somehow associated with lumen opening in the *Ciona* notochord (20, 41).

As previously described (20), the myosin regulatory light chain fused to EGFP (MRLC:EGFP) showed accumulation in the basal contractile ring (Movie S12). Extending these previous observations, we found that, during phase II (15 to 17 hpf), myosin II showed dynamic cycles of pulsatile accumulation in the basal contractile ring, followed by directed basal–apical flows through the cytoplasm (Fig. 6). Using two-color live imaging, we found that basal accumulation and basal–apical movements of myosin II were tightly coordinated with those of 14-3-3εa and ERM (Fig. 6 and Movie S12). These observations suggest that local interactions between 14-3-3εa and ERM control pulsatile accumulation and directed transport not just of themselves, but also of other cortically associated factors.

Discussion

Studies of *Ciona* notochord tubulogenesis have focused mainly on candidate genes that are highly expressed in notochord cells or during tubulogenesis in other organisms. In this study, we took

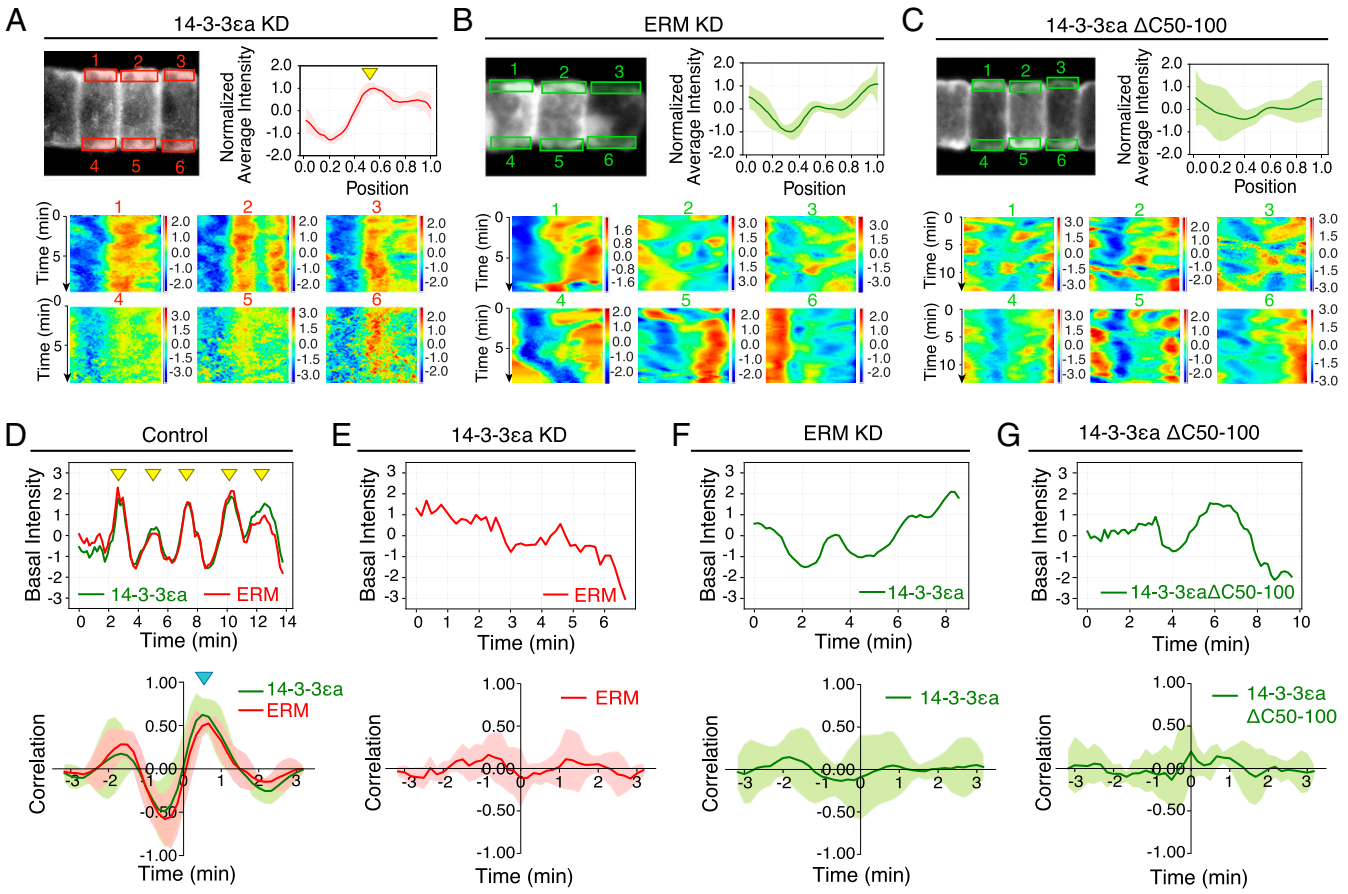

Fig. 5. Loss of the pulsatile basal accumulation and basal–apical translocation by the inhibition of 14-3-3εa–ERM interaction. (*A–C*) Kymographs for the live images of mCherry:ERM in a 14-3-3εa KD larva (*A*), 14-3-3εa:EGFP in an ERM KD larva (*B*), and 14-3-3εaΔC50-100:EGFP in a 14-3-3εa KD larva at 15 hpf (*C*). The intensities in the ROI (shown in red or green rectangles) were quantified, normalized along the AP axis, and displayed as a kymograph. The total intensities of all ROIs and time points were plotted along relative position of the AP axis. The yellow arrowhead indicates the accumulation of mCherry:ERM in the basal contractile ring, the middle position of the basal domain. (*D–G*) The basal ring intensity over time during phase II (15 to 17 hpf, *Upper*) and the cross-correlation analysis between the intensities of the basal contractile ring and the apical domain (*Lower*). Yellow arrowheads indicate their pulsatile accumulation in the basal contractile ring. The blue arrowhead indicates the peak, the shift of which indicates a high correlation between the basal contractile ring and the apical domain. (*D*) Larva injected with control MO; (*E*) larva injected with 14-3-3εa MO; (*F*) larva injected with ERM MO; and (*G*) larvae expressing 14-3-3εaΔC50-100:EGFP under 14-3-3εa MO.

an in vivo chemical genetics approach to identify genes that are responsible for *Ciona* notochord tubulogenesis. This in vivo chemical genetics approach led us to identify UTKO1 to be a selective inhibitor of notochord tubulogenesis (Fig. 1), to identify its target 14-3-3εa, and gain functional insights into 14-3-3εa's role in notochord tubulogenesis.

Because UTKO1 has been reported to inhibit tumor cell migration by targeting 14-3-3ζ, we examined the possibility that UTKO1 also binds to *Ciona* 14-3-3. Our in vitro binding assay clearly showed that, among four 14-3-3 isoforms in *Ciona*, UTKO1 selectively binds to 14-3-3εa through its 156- to 206-aa domain (Figs. 2*D* and 3 *D* and *E*). Furthermore, 14-3-3εa KD resulted in failed lumen formation in the notochord (Fig. 2 *G–J*), a similar phenotype to that observed following UTKO1 treatment. Therefore, our in vivo chemical genetics approach enabled us to identify 14-3-3εa as a molecule responsible for *Ciona* notochord tubulogenesis.

The 14-3-3 proteins are thought to exert their roles as adapter proteins that interact with various kinds of client proteins. Here, we have identified *Ciona* ERM as a client protein through which 14-3-3εa exerts its effects on notochord tubulogenesis. *Ciona* ERM is required for lumen formation (20) and is predominantly expressed in the notochord (38, 39). In human cell lines, ezrin interacts with 14-3-3ζ to regulate cell migration (40). Indeed, we found that 14-3-3εa interacted directly with ERM (Fig. 3*B*) and colocalized with ERM in the basal contractile ring (Fig. 3*G*). Although we cannot fully rule out other possibilities, the inhibitory effects of UTKO1 toward direct 14-3-3εa–ERM interaction (Fig. 3*B*), their colocalization (Fig. 3 *G* and *H*), and their dynamics (Fig. 4 *B–I*) strongly suggest the involvement of ERM as a 14-3-3εa client protein responsible for the early stage of *Ciona* notochord tubulogenesis.

Our live imaging analysis of 14-3-3εa and ERM revealed fundamental insights into their roles in lumen formation. Before lumen opening, 14-3-3εa and ERM were stably coenriched in a basal actomyosin ring (Fig. 4*A*). However, during lumen opening and growth, we found that 14-3-3εa and ERM undergo repeated cycles of accumulation in the basal contractile ring, followed by rapid translocation from the basal surface toward the lumen-facing apical domain (Fig. 4*H* and Movie S3). These movements were tightly correlated with movements of myosin II (Fig. 6) and other cytoplasmic elements toward the apical surface (Fig. 4*L*), suggesting that they are carried as part of a bulk flow of material from the basal surface to the apical lumen (Fig. 4*L* and Movie S3). Importantly, neither pulsatile basal accumulation, nor directed basal–apical transport, nor lumen formation were observed when the 14-3-3εa–ERM interaction was destroyed by pharmacological or genetic methods

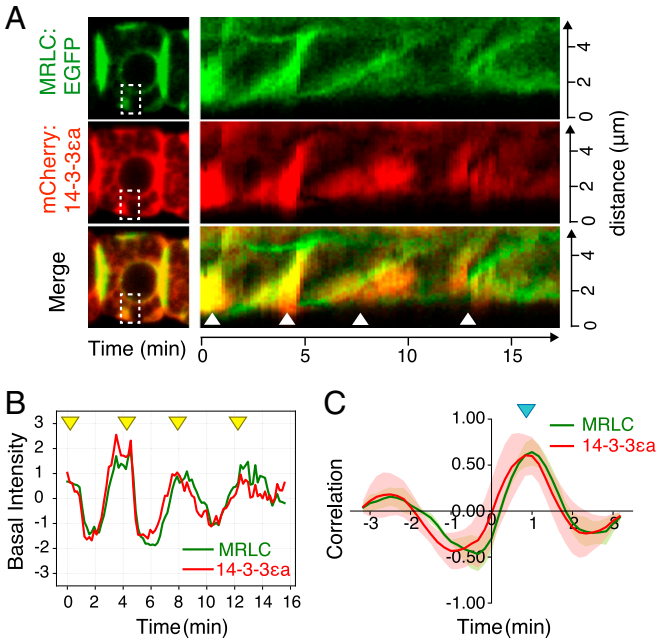

Fig. 6. Translocation of myosin II toward the apical domain together with 14-3-3εa. (*A*) Kymograph analysis of the dynamics of myosin II (MRLC) and 14-3-3εa (mCherry:14-3-3εa), and their merging during phase II (15 to 17 hpf). The placement of the cross-sections used to generate the kymograph is indicated by white dashed lines. White triangles indicate the pulsed accumulation of MRLC and 14-3-3εa. (*B*) The intensity of MRLC and 14-3-3εa in the basal contractile ring over time. Yellow arrowheads indicate the pulsatile accumulation of MRLC and 14-3-3εa. (*C*) Cross-correlation analysis between the intensities of the basal contractile ring and apical domain for myosin II and 14-3-3εa. The blue arrowhead indicates the peak, the shift of which indicates a highest correlation between the basal contractile ring and the apical domain.

[UTKO1 (Fig. 4 *D*–*I* and Movie S4); 14-3-3εa KD (Fig. 5*E* and Movie S9); ERM KD (Fig. 5*F* and Movie S10); and 14-3-3εaΔC50-100 (Fig. 5*G* and Movie S11)]. These findings suggest that the 14-3-3εa–ERM interaction plays a key role in lumen formation by directing transport of factors required for lumen growth to the apical surface (Fig. 7).

The mechanisms by which 14-3-3εa–ERM governs pulsatile accumulation of basal factors and their subsequent transport toward the apical surface of the growing lumen remain unclear. An attractive possibility is that 14-3-3εa–ERM act by regulating pulsatile actomyosin contractility and cortical flow (42, 43). Previous studies described the recruitment of myosin II to the basal contractile ring via cortical flows directed from cell–cell contacts toward the ring (22). Our observations are consistent with the possibility that pulsatile contraction and flow of cortical actomyosin II drive accumulation of both myosin II and 14-3-3εa–ERM in the basal contractile ring (Fig. 6*B*). In principle, actomyosin contractility could also drive their detachment from the membrane; a contraction of cytoplasmic actomyosin could drive their basal–apical transport through the cytoplasm. ERM proteins are known to tether the actomyosin network directly to the plasma membrane and to regulate cortical tension and flow in other contexts (44–48). The 14-3-3 proteins can also associate with myosin II to regulate cortical tension and flow (49–52). The observation that pulsatile basal accumulation of 14-3-3εa–ERM and their subsequent basal–apical translocation are abolished by removing either protein or preventing their interactions [UTKO1 (Fig. 4 *D*–*I* and Movie S4); 14-3-3εa KD (Fig. 5*E* and Movie S9); ERM KD (Fig. 5*F* and Movie S10); and 14-3-3εaΔC50-100 (Fig. 5*G* and Movie S11)] is consistent with the idea that 14-3-3εa–ERM interact to promote actomyosin contractility and raises the intriguing possibility that pulsatile contraction of the basal cortex and transient apical–basal flows could be coupled through local regulation of actomyosin contractility by 14-3-3εa–ERM.

Our findings reveal a key role for 14-3-3εa–ERM in lumen formation (Fig. 7). The basal contractile ring also plays crucial roles in cell elongation along the AP axis (20, 22, 53), which may explain the short-tail phenotype caused by UTKO1 (*SI Appendix*, Fig. S1*B*). In *Ciona* and other tubulogenesis processes, cell elongation and lumen formation are closely related (20, 54, 55). Thus, by promoting both basal contraction and cortical flow, and basal–apical cytoplasmic flow, 14-3-3εa–ERM in the basal contractile ring would play roles in both cell elongation and lumen formation. Until now, lumen formation in the *Ciona* notochord has mainly been investigated by focusing on apically localizing molecules, such as Par-3/Par-6/aPKC or Slc26aα, as well as ERM itself. Studies of the mechanisms of basal contractility and directed flow are needed to provide molecular or mechanical insights into tubulogenesis, bridging the gap between these two opposite domains.

Materials and Methods

Biological Materials. *C. intestinalis* were cultivated in Maizuru (Kyoto), Misaki (Kanagawa), and Shinyamasita (Kanagawa). Adults were maintained under constant light to induce oocyte maturation. Eggs and sperm were obtained by dissecting the gonadal and sperm ducts, respectively. Eggs were dechorionated using a dechorionation reagent containing 0.05% Actinase E (Kaken Pharmaceutical) and 1% mercaptoacetic acid sodium salt (Wako Pure Chemical Industries) in sea water, and cross-fertilization was performed in plastic Petri dishes. After fertilization, embryos were cultured at 18 °C. The onset of notochord tubulogenesis was at ∼12 hpf.

Chemicals and Antibodies. UTKO1 and its analogs were synthesized as previously described (32, 33) and dissolved in methanol. Biotin was purchased from Sigma-Aldrich. The 14-3-3εa and ERM antibodies were purchased from and produced by Biologica Co. Ltd using the short peptides "EQMKKIAQLGISLT" (for 14-3-3εa) and "KQIRSGNTKHRIDEFEC" (for ERM) to immunize rabbits and chickens, respectively. GST and a-pan-14-3-3 antibody

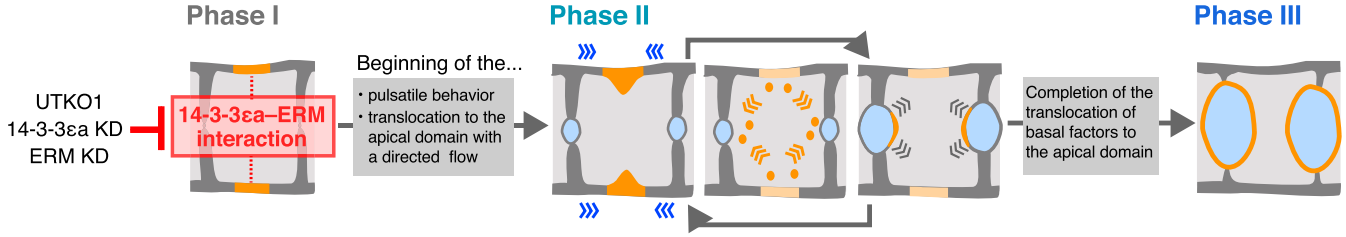

Fig. 7. Proposed models of lumen formation in *Ciona* notochord tubulogenesis via the interaction of 14-3-3εa and ERM. Orange coloring indicates basal factors, including 14-3-3εa, ERM, myosin II, and other cytoplasmic elements. Blue arrowheads indicate cortical flows at the basal surface, directed toward the basal equator, which would enable pulsatile accumulation in the basal contractile ring. Orange arrowheads indicate a directed flow through the cytoplasm from the basal cortex toward the lumen-adjacent apical domain. Gray arrowheads indicate the alteration of the lumen architecture.

were purchased from Santa Cruz Biotechnology, and His and GFP antibody were obtained from Clontech.

Imaging. Confocal images for phalloidin staining were prepared as previously described (31). For the immunostaining analysis, *Ciona* larvae were fixed with 10% formalin in seawater for 30 min. They were washed several times with 0.1% Triton-X in PBS (PBST) and blocked with 10% donkey serum in PBST for 2 h. The antibody for 14-3-3εa and ERM was added, and the samples were incubated for 2 h. After several washes in PBST, larvae were incubated with the second antibody for 2 h and again washed several times in PBST. For 14-3-3εa and GFP staining, the signal was amplified using Tyramide SuperBoost Kits with Alexa Fluor Tyramides (Invitrogen), according to the manufacturer's instructions. These specimens were photographed using a confocal laser scanning microscope system FV1000 (Olympus). Live imaging was performed by fixing living *Ciona* larvae with 2% Agarose-LM Sieve (nacalai tesque) in seawater.

Image Processing and Quantification. We used the open-source program Fiji to perform all basic image-processing tasks, to quantify the average signal intensities of the region of interest (ROI), to measure the size of the ROI, and to calculate the correlation coefficient for the colocalization tests. In live imaging, the TurboReg plugin was used to register frames to prevent the apparent blurring of the images. To generate kymographs with a heat map in live imaging, the intensities in the basal domain surrounded by the ROIs were quantified and normalized along the AP axis for every time point. Subsequently, kymographs were generated by Fiji. Finally, colors were annotated using the Python programming language to generate the heat map, showing a gradient color scale from red, indicating relatively high intensity, to blue, indicating relatively low intensity. To conduct a cross-correlation analysis, ROIs for the basal contractile ring and the apical domain were manually set for each period (200 s), and their cross-correlation was calculated with MATLAB (MathWorks).

Plasmid Construction. The 14-3-3 proteins (εa, εb, γ1, and γ2) were amplified by PCR from a cDNA library, using a pair of primers containing the FLAG tag sequence: 5′-CGCGGATCCCTGATTACAAGGATGACGACGATAAGATGTCTACTGAGCGCGAGGA-3′ and 5′-CCGGAATTCTCTAGATTATGACGCTTCAGTGGCAT-3′ for 14-3-3εa; 5′-CGCGGATCCCTGATTACAAGGATGACGACGATAAGATGTCTACTGAACGTGAAGA-3′ and 5′-CCGGAATTCTCTAGATTAAGGCTCATCATTTGCAT-3′ for 14-3-3εb; 5′-CGCGGATCCCTGATTACAAGGATGACGACGATAAGATGTCGTCAAGAGAAGACAT-3′ and 5′-CGCGGATCCTTAATCTTCAGTGTCCTGTA-3′ for 14-3-3 γ1; and 5′-CCGGAATTCAGATTACAAGGATGACGACGATAAGATGGCTGACGATCGTGATAC-3′ and 5′-CCGGAATTCTCTAGACTAATCCTCACACTGCGGGT-3′ for 14-3-3 γ2. These were cloned into pGEX-3X (GE Healthcare) or pRSET-C (Invitrogen) to prepare GST or His fusion 14-3-3 proteins in *E. coli*. ERM was obtained from Bra>ERM:EGPF, EGFP fusion ERM protein with Brachyury promoter (39), and cloned into pCold-I to prepare the expression plasmids for the His fusion ERM protein in *E. coli*. To prepare Bra>14-3-3εa:EGFP, Bra>14-3-3εa:mCherry, and Bra>mCherry:ERM, the sequences for 14-3-3εa and ERM were introduced to Bra>EGFP (39) and Bra>mCherry, which was modified from Bra>EGFP. The 14-3-3εa MO-resistant expression plasmids were prepared by introducing mutations in Bra>14-3-3εa:EGFP using the following primers: 5′-ATGAGCACAGAACGCGAGGACTTTGTA-3′ and 5′-GCGTTCTGTGCTCATCTGCAGAATTCG-3′. Myosin II was amplified from *Ciona* cDNA using a pair of primers (5′-CCGGAGGTACCGATGTCGAGCCGACGAACT-3′ and 5′-CCGGAGGATCCTTAATGTCATCTTTTTCTT-3′) and was ligated into Bra>EGFP to obtain Bra>MRLC:EGFP.

In Vitro Biotin-UTKO1 Pull-Down Assay and Western Blotting. Lysates of *Ciona* larvae at 15 hpf, or GST fusion proteins, which were expressed in the *E. coli* BL21 strain and purified using Glutathione Sepharose 4B (GE Healthcare), were incubated with B-UTKO1ox/B-UTKO1ph and avidin beads in immunoprecipitation (IP) buffer (50 mM Hepes, pH 7.5, 150 mM NaCl, 1 mM EDTA, 2.5 mM EGTA, 1 mM DTT, 10% glycerol, and protease inhibitor mixture). The beads were washed with IP buffer and PBS and eluted with 2 mM biotin in PBS, all at 4 °C. The eluted proteins were subjected to SDS/PAGE. Proteins were detected using an ECL Western blotting system (Millipore) and an LAS-1000 CCD camera (Fujifilm) or the ChemiDoc XRS+ System (Bio-Rad). For the competition assay, UTKO1 was added before incubating the samples with B-UTKO1ox.

Microinjection of Morpholino Oligonucleotide. Morpholino antisense oligonucleotides (MOs) were purchased from Gene Tools, LLC: 5′-CAAAGTCCTCGCGCTCAGTAGACAT-3′ for 14-3-3εa and 5′-GTTTCCAAACATTATTACATCACAG-3′ for ERM. The unfertilized eggs were injected with a mixture of 0.5 mM MO and Fast Green or Phenol red as dye. A standard control MO from GeneTools was used as a negative control.

Binding Assay for ERM and 14-3-3 Proteins. GST-14-3-3εa (50 pmol) was incubated with or without UTKO1/UTKO10 for 1 h, incubated with His-ERM (100 pmol) in 300 μL of IP buffer for 2 h, and incubated with cOmplete His-tag purification resin (Roche) for 30 min. Beads were washed three times with IP buffer and eluted with an elution buffer containing 250 mM imidazole in IP buffer. Eluted proteins were subjected to SDS/PAGE.

ACKNOWLEDGMENTS. We thank the National Bio-Resource Project for providing the *Ciona*. We thank Dr. Hiroki Takahashi (National Institute for Basic Biology) for the Bra>ERM:EGFP plasmids; Dr. Akira Funahashi (Keio University) for helpful discussion about imaging analysis; and Dr. Edwin Munro (University of Chicago) for helpful discussion and reviewing the manuscript. This work was supported by a Grant-in-Aid for Scientific Research (C) (Grant JP16K07426 to K.H.), a Grant-in-Aid for Challenging Exploratory Research (Grant JP25560419 to M.I.), and Grant-in-Aid for Scientific Research in Innovative Areas (Grants JP23102006 and JP17H06401 to M.I. and JP16H01451 to K.H.) from The Ministry of Education, Culture, Sports, Science and Technology; and a Grant-in-Aid from Japan Society for the Promotion of Science (Grant JP16J04182 to Y.M.).

1. Dong B, et al. (2009) Tube formation by complex cellular processes in Ciona intestinalis notochord. *Dev Biol* 330:237–249.
2. Strilić B, et al. (2009) The molecular basis of vascular lumen formation in the developing mouse aorta. *Dev Cell* 17:505–515.
3. Khan LA, et al. (2013) Intracellular lumen extension requires ERM-1-dependent apical membrane expansion and AQP-8-mediated flux. *Nat Cell Biol* 15:143–156.
4. JayaNandanan N, Mathew R, Leptin M (2014) Guidance of subcellular tubulogenesis by actin under the control of a synaptotagmin-like protein and Moesin. *Nat Commun* 5:3036.
5. Alvers AL, Ryan S, Scherz PJ, Huisken J, Bagnat M (2014) Single continuous lumen formation in the zebrafish gut is mediated by smoothened-dependent tissue remodeling. *Development* 141:1110–1119.
6. Bryant DM, et al. (2010) A molecular network for de novo generation of the apical surface and lumen. *Nat Cell Biol* 12:1035–1045.
7. Li D, Kuehn EW, Prekeris R (2014) Kinesin-2 mediates apical endosome transport during epithelial lumen formation. *Cell Logist* 4:e28928.
8. Chou S-Y, et al. (2016) CLIC4 regulates apical exocytosis and renal tube luminogenesis through retromer- and actin-mediated endocytic trafficking. *Nat Commun* 7:10412.
9. Wehman AM, Poggioli C, Schweinsberg P, Grant BD, Nance J (2011) The P4-ATPase TAT-5 inhibits the budding of extracellular vesicles in C. elegans embryos. *Curr Biol* 21:1951–1959.
10. Armenti ST, Chan E, Nance J (2014) Polarized exocyst-mediated vesicle fusion directs intracellular lumenogenesis within the C. elegans excretory cell. *Dev Biol* 394:110–121.
11. Kato K, et al. (2016) Microtubule-dependent balanced cell contraction and luminal-matrix modification accelerate epithelial tube fusion. *Nat Commun* 7:11141.
12. Göbel V, Barrett PL, Hall DH, Fleming JT (2004) Lumen morphogenesis in C. elegans requires the membrane-cytoskeleton linker erm-1. *Dev Cell* 6:865–873.
13. Saotome I, Curto M, McClatchey AI (2004) Ezrin is essential for epithelial organization and villus morphogenesis in the developing intestine. *Dev Cell* 6:855–864.
14. Kamei M, et al. (2006) Endothelial tubes assemble from intracellular vacuoles in vivo. *Nature* 442:453–456.
15. Mangan AJ, et al. (2016) Cingulin and actin mediate midbody-dependent apical lumen formation during polarization of epithelial cells. *Nat Commun* 7:12426.
16. Munro EM, Odell GM (2002) Polarized basolateral cell motility underlies invagination and convergent extension of the ascidian notochord. *Development* 129:13–24.
17. Munro EM, Odell G (2002) Morphogenetic pattern formation during ascidian notochord formation is regulative and highly robust. *Development* 129:1–12.
18. Shi W, Peyrot SM, Munro E, Levine M (2009) FGF3 in the floor plate directs notochord convergent extension in the Ciona tadpole. *Development* 136:23–28.
19. Jiang D, Smith WC (2007) Ascidian notochord morphogenesis. *Dev Dyn* 236:1748–1757.
20. Dong B, Deng W, Jiang D (2011) Distinct cytoskeleton populations and extensive crosstalk control Ciona notochord tubulogenesis. *Development* 138:1631–1641.
21. Veeman MT, McDonald JA (2016) Dynamics of cell polarity in tissue morphogenesis: A comparative view from Drosophila and Ciona. *F1000Res* 5:1084.
22. Sehring IM, et al. (2014) An equatorial contractile mechanism drives cell elongation but not cell division. *PLoS Biol* 12:e1001781.
23. Denker E, Bocina I, Jiang D (2013) Tubulogenesis in a simple cell cord requires the formation of bi-apical cells through two discrete Par domains. *Development* 140:2985–2996.
24. Apodaca G, Gallo LI, Bryant DM (2012) Role of membrane traffic in the generation of epithelial cell asymmetry. *Nat Cell Biol* 14:1235–1243.
25. Datta A, Bryant DM, Mostov KE (2011) Molecular regulation of lumen morphogenesis. *Curr Biol* 21:R126–R136.

26. Van Fürden D, Johnson K, Segbert C, Bossinger O (2004) The C. elegans ezrin-radixin-moesin protein ERM-1 is necessary for apical junction remodelling and tubulogenesis in the intestine. *Dev Biol* 272:262–276.
27. Schreiber SL (1998) Chemical genetics resulting from a passion for synthetic organic chemistry. *Bioorg Med Chem* 6:1127–1152.
28. Stockwell BR (2000) Chemical genetics: Ligand-based discovery of gene function. *Nat Rev Genet* 1:116–125.
29. Murphey RD, Stern HM, Straub CT, Zon LI (2006) A chemical genetic screen for cell cycle inhibitors in zebrafish embryos. *Chem Biol Drug Des* 68:213–219.
30. Tan JL, Zon LI (2011) Chemical screening in zebrafish for novel biological and therapeutic discovery. *Methods Cell Biol* 105:493–516.
31. Hotta K, et al. (2007) A web-based interactive developmental table for the ascidian Ciona intestinalis, including 3D real-image embryo reconstructions: I. From fertilized egg to hatching larva. *Dev Dyn* 236:1790–1805.
32. Sawada M, et al. (2011) Synthesis and anti-migrative evaluation of moverastin derivatives. *Bioorg Med Chem Lett* 21:1385–1389.
33. Kobayashi H, et al. (2011) Involvement of 14-3-3 proteins in the second epidermal growth factor-induced wave of Rac1 activation in the process of cell migration. *J Biol Chem* 286:39259–39268.
34. Muslin AJ, Tanner JW, Allen PM, Shaw AS (1996) Interaction of 14-3-3 with signaling proteins is mediated by the recognition of phosphoserine. *Cell* 84:889–897.
35. Yaffe MB, et al. (1997) The structural basis for 14-3-3:phosphopeptide binding specificity. *Cell* 91:961–971.
36. Satou Y, Kawashima T, Shoguchi E, Nakayama A, Satoh N (2005) An integrated database of the ascidian, Ciona intestinalis: Towards functional genomics. *Zool Sci* 22: 837–843.
37. Kusakabe T, et al. (2002) Gene expression profiles in tadpole larvae of Ciona intestinalis. *Dev Biol* 242:188–203.
38. Hotta K, et al. (2000) Characterization of Brachyury-downstream notochord genes in the Ciona intestinalis embryo. *Dev Biol* 224:69–80.
39. Hotta K, Yamada S, Ueno N, Satoh N, Takahashi H (2007) Brachyury-downstream notochord genes and convergent extension in Ciona intestinalis embryos. *Dev Growth Differ* 49:373–382.
40. Chen M, et al. (2014) Direct interaction of 14-3-3ζ with ezrin promotes cell migration by regulating the formation of membrane ruffle. *J Mol Biol* 426: 3118–3133.
41. Denker E, et al. (2015) Regulation by a TGFβ-ROCK-actomyosin axis secures a non-linear lumen expansion that is essential for tubulogenesis. *Development* 142: 1639–1650.
42. Munro E, Nance J, Priess JR (2004) Cortical flows powered by asymmetrical contraction transport PAR proteins to establish and maintain anterior-posterior polarity in the early C. elegans embryo. *Dev Cell* 7:413–424.
43. Murrell M, Oakes PW, Lenz M, Gardel ML (2015) Forcing cells into shape: The mechanics of actomyosin contractility. *Nat Rev Mol Cell Biol* 16:486–498.
44. Salbreux G, Charras G, Paluch E (2012) Actin cortex mechanics and cellular morphogenesis. *Trends Cell Biol* 22:536–545.
45. Ramkumar N, Baum B (2016) Coupling changes in cell shape to chromosome segregation. *Nat Rev Mol Cell Biol* 17:511–521.
46. Rouven Brückner B, Pietuch A, Nehls S, Rother J, Janshoff A (2015) Ezrin is a major regulator of membrane tension in epithelial cells. *Sci Rep* 5:14700.
47. Liu Y, et al. (2012) Constitutively active ezrin increases membrane tension, slows migration, and impedes endothelial transmigration of lymphocytes in vivo in mice. *Blood* 119:445–453.
48. Fievet BT, et al. (2013) Systematic genetic interaction screens uncover cell polarity regulators and functional redundancy. *Nat Cell Biol* 15:103–112.
49. Zhou Q, et al. (2010) 14-3-3 coordinates microtubules, Rac, and myosin II to control cell mechanics and cytokinesis. *Curr Biol* 20:1881–1889.
50. Cheeks RJ, et al. (2004) C. elegans PAR proteins function by mobilizing and stabilizing asymmetrically localized protein complexes. *Curr Biol* 14:851–862.
51. Munro EM (2006) PAR proteins and the cytoskeleton: A marriage of equals. *Curr Opin Cell Biol* 18:86–94.
52. Basant A, et al. (2015) Aurora B kinase promotes cytokinesis by inducing centralspindlin oligomers that associate with the plasma membrane. *Dev Cell* 33:204–215.
53. Sehring IM, et al. (2015) Assembly and positioning of actomyosin rings by contractility and planar cell polarity. *eLife* 4:e09206.
54. Gervais L, Casanova J (2010) In vivo coupling of cell elongation and lumen formation in a single cell. *Curr Biol* 20:359–366.
55. Dong B, Kakihara K, Otani T, Wada H, Hayashi S (2013) Rab9 and retromer regulate retrograde trafficking of luminal protein required for epithelial tube length control. *Nat Commun* 4:1358.